Models for solidification and splashing in laser percussion drilling

Warren R. Smith[1]
Department of Mathematics and Computing Science, Technische Universiteit Eindhoven, PO Box 513, 5600 MB Eindhoven, The Netherlands

Abstract. This paper studies systems of partial differential equations modelling laser percussion drilling. The particular phenomenon considered in detail is the ejection of the thin layer of molten material. This thin layer is modelled as an inviscid flow between the fluid surface and fluid/solid interface, both of which are unknown moving boundaries. Through a regular asymptotic expansion, the governing equations are reduced to a combination of the shallow water equations in the zero gravity limit and a two-phase Stefan problem; the key small parameter being the square of the aspect ratio. These leading-order problems exhibit shocks which represents a possible mechanism for the previously unexplained fluid clumping. Approximate formulas and a parameter grouping are derived to predict the rate of melt solidification during ejection. Finally, weak formulations of the convection-diffusion equation for energy conservation are presented. These weak formulations are novel because the fluid is moving across a solid surface. An appropriate extension to the enthalpy method is suggested as a first stage towards numerical calculations.

Keywords. laser percussion drilling, mathematical modelling, weak formulations

AMS(MOS) subject classifications. 35R35, 80A22

1 Introduction

Laser percussion drilling is used to machine gas turbine components which are typically made out of superalloys; these materials cannot be machined with conventional mechanical drills. The term percussion refers to the repeated operation of the laser in short pulses (10^{-3}s) which are separated by longer time periods (10^{-2}s). The laser builds up energy at a bounded rate and operation in this manner allows for large bursts of energy. Percussion drilling is favoured over other processes, such as spark erosion drilling or laser trepanning drilling, because it is by far the quickest. However, it suffers from three drawbacks (i) recast of solidified material at the wall of the hole, (ii) tapering, that is the decrease of hole diameter with depth and (iii) bellow shape, that is the local increase of hole diameter. Experimental results have also shown that the penetration depth is limited.

In laser percussion drilling, the metal is ablated by a combination of evaporation and melt ejection. However, the mass fraction extracted by evaporation is typically less than a tenth of the total mass loss [1, p. 133]. The melt ejection can be split into three different stages, shown in Figure 1. Initially a thin region of molten metal is formed by the absorption of laser energy at the target surface. This thin molten region at the base of the hole is known as the melt pool. Eventually, the irradiated surface reaches the vaporisation temperature. A splash occurs in which the molten metal is pushed radially by the pressure gradients generated by the sudden expansion of the vapour evaporating from the surface (see the photographs of the early stages of melt ejection [1, p. 133]). The high recoil pressures involved also cause significant variation in the vaporisation temperature and rapid flow of the vapour and air away from the irradiated surface. The molten metal now has a high velocity and it can escape from the hole. However, this liquefied material can resolidify before it

[1]Current address: School of Mathematics and Statistics, The University of Birmingham, Edgbaston, Birmingham, B15 2TT, UK (smithwar@maths.bham.ac.uk).

escapes from the hole. The walls of the hole are relatively cold and large temperature gradients occur across the thin film. The solid metal left exposed after the splash now starts to absorb laser energy and so on. The time-scales for these three stages are between 10^{-5} s and 10^{-4}s for melting, and 10^{-5}s for splashing and solidification. We therefore expect between 10 and 100 splashes within a 10^{-3}s pulse. In this paper, we will be concerned with developing models for solidification of the thin film as it moves along the side wall of the hole, and splashing at the base of the hole.

A series of photographs of a hole machined by laser percussion drilling is shown in Figure 2. The number denotes the number of pulses used to create the hole. The growth rate of the hole is initially constant but slows in the later photographs. The eleventh hole appears to be not as deep as the tenth, because the melt pool has solidified at the base of the hole in such a way as to obscure the base. The melt pool has probably solidified at the base of the hole because the pulse ended before the splash had been completed. We note that the seventh and subsequent photographs show the resolidified material on the wall of the hole. This resolidification may be in the form of very thin layers, or more irregular clumps. In the last three photographs molten metal will have escaped via the bottom exit. There may be variability in the laser characteristics, in particular the radial, azimuthal and temporal intensity profile; this making repeatability of experimental results very difficult, even with an identical set-up.

The subject of laser percussion drilling has been studied by several authors (see [6] and references therein). The fluid is modelled by the incompressible Navier-Stokes equations including gravity. These equations are currently exclusively solved by numerical approaches, which require extensive computing resources [7]. In this paper, we employ perturbation methods to simplify the models retaining only the most significant physical effects. In particular, we note that the depth of the melt pool is typically of the order of 10^{-4}m (which is determined by a balance between heat flux and laser intensity at the surface of the melt pool, that is $k(T_v - T_m)/I_t \sim 10^{-4}$m where I_t is the typical laser intensity and the other parameters are given in Table 1) whereas the radius is typically of the order of 10^{-3}m. We will take full advantage of this small aspect ratio.

In the process of melt ejection the Reynolds number is typically much greater than 10^3; the typical values being described below. Such flows undergo a transition to turbulence when the flow has developed. It is unclear and not trivial to determine experimentally at what length-scale this transition will take place. The developed turbulent fluid flow consists of eddies of many different scales. It is common practice to use empirical models to describe such flows (see, for example, river flow [4, p. 254]). However, we use a thin-film approximation to inviscid irrotational flow to derive a simplified model similar to the well-established shallow water equations. The leading-order problems also incorporate a two-phase Stefan problem (see [3]). The equations developed in the inviscid limit of laminar flow, which represent conservation of mass, momentum and energy, will be assumed to also describe the averaged behaviour of the developed turbulent flow. We do not incorporate a friction law; this being discussed below.

Once the transition to turbulence has taken place, it would be appropriate to use an effective thermal diffusivity rather than the material thermal conductivity. As it is unclear at what point the parameters are modified, we make the simplifying assumption that the (constant) thermal conductivity forms a reasonable approximation in this article. The effective thermal diffusivity may be replaced in the calculations at a later stage if it is found to improve the agreement with experiments.

In the absence of experimental data, it is not possible to say whether or not the superalloys under consideration melt and solidify over a range of temperatures. The laser percussion drilling of aluminium will be considered here; aluminium being known to have a single melting point. Therefore, mushy regions will not be considered.

The purpose of this paper is to gain a better understanding of the process of laser percussion drilling. We derive a variety of models for the splash and the melt ejection immediately following the splash. The eventual aim is to select parameters to minimise the three drawbacks associated with laser percussion drilling.

The process depends on the material properties, ambient conditions and laser characteristics. However, as well as analysing laser percussion drilling we note that the solidification problem described below is an open problem in the fluid mechanics of lava flow of finite extent (see the penultimate paragraph in the conclusions of [8]). In the case of lava flow it may not be possible to neglect gravity in comparison to inertia, so that the solidification model may require minor modification. The extension of the enthalpy method described below is the required technique to deal with the situation in which the solidification will engulf the flow. The extension of the enthalpy method we develop will also carry over to the solidification of thin drops using a lubrication approximation.

The contents of the paper will now be outlined. The dimensionless parameters are calculated in Section 2. Mathematical models for solidification and splashing are then formulated on the basis of the parameter values. Through a regular asymptotic expansion, the leading-order problems are derived in Section 3; the small parameters being the square of the aspect ratio and the reciprocal of the Stefan number for vaporisation. The physical problem contains coupled moving boundaries, however, the leading-order problem incorporates a differential equation for the free fluid surface with only the thermal equation remaining as a field equation. Shocks occur and appropriate Rankine-Hugoniot relations are deduced. Section 4 describes two approximate analytical solutions to the leading-order problem for solidification: a similarity transformation in the large-time limit (corresponding to deep holes) and a singular asymptotic expansion in the limit of small diffusion. We determine that in the absence of shocks, other than the leading-edge shock, the resolidified material may grow in thin layers in the large-time limit. In the case of small diffusion, an analytical expression for the growth of the resolidification is obtained. In Section 5, weak formulations for the conservation of energy equations are deduced which are consistent with the Stefan condition at the fluid/solid interface. These weak formulations are unusual because the fluid is moving across a solid surface. An appropriate extension to the enthalpy method is suggested as a first stage towards numerical calculations. Finally, Section 6 gives a brief discussion of the results.

2 Problem formulation

2.1 Parameter régimes

The different parameters in the model depend on laser set-up, the material to be drilled and the local fluid temperature, which for aluminium may vary from 300K to approximately 2500K. For the drilling of aluminium the parameters are given in Table 1 (see, for example, [14]). With a length-scale of $L \sim 10^{-3}$m and thickness $d \sim 10^{-4}$m, a typical aspect ratio is given by $\delta = d/L \sim 0.1$. Of course the aspect ratio changes considerably during the ejection of the melt and the variation in viscosity can result in deviation in the Reynolds number. With a typical maximum velocity given by $U \sim 50\text{ms}^{-1}$ (see [1, p. 132]), the dimensionless parameters are

$$Re = \frac{\rho U L}{\mu} \sim 5 \times 10^4, \quad Fr = \frac{U^2}{Lg} \sim 3 \times 10^5, \quad Pe = \frac{\rho c U L}{k} \sim 5 \times 10^2,$$

$$Br = \frac{\mu U^2}{k(T_v - T_m)} \sim 2 \times 10^{-5}, \quad We = \frac{\rho U^2 L}{\sigma} \sim 7 \times 10^3,$$

where g is the acceleration due to gravity. The order of the parameters motivates us to consider inviscid flow with heat convection and conduction, neglecting viscous boundary layers, surface tension and gravity. Moreover, we assume that the vorticity is initially zero, so that we may consider irrotational flow.

There are very short length-scales sufficiently close to the leading edge of a drop of compact support where viscosity and surface tension are significant. This region has no effect on the body of the flow because information propagates towards the leading edge (the characteristic speeds of the shallow water equations in the zero gravity limit are both positive).

We do not incorporate a friction law despite the possibility of turbulence developing. We estimate the order of magnitude of the wall shear stress to be $f\rho U^2/8$ where we adopt the Blasius friction factor $f = 0.316Re^{-1/4}$ (see [9]). Therefore the relative importance of wall shear stress in relation to inertia is given by

$$\left(\frac{f\rho U^2}{8}\right) / \left(\frac{\rho U^2 d}{L}\right) \sim 10^{-2}$$

This indicates the melt is not retained in the hole due to momentum loss, but by solidification.

The three stages in the melt ejection described above and shown in Figure 1 are (i) melt-pool formation, (ii) a splash in which the melt pool is accelerated out of the base of the hole and (iii) the solidification process in which the hot fluid is moving across the cold side wall of the drilled hole. (i) The model for the melt-pool formation is conventional as there is no fluid motion and we will not discuss it. (ii) In the splashing model, we make the simplifying assumption that the entire fluid surface is at vaporisation temperature. However, it may well be the case that only a fraction of the fluid surface is at vaporisation temperature and a mixed boundary value problem must then be studied. The base of the drilled hole is idealised as an axisymmetric geometry as shown in Figure 3. The axial coordinate is along the axis of the drilled hole and the radial coordinate is across the radius of the base of the drilled hole. (iii) Once the fluid has moved away from the base of the hole, it is no longer accelerated. There is competition between inertia and solidification as a fluid ring moves up the cold side wall of the drilled hole. The radius of curvature of the melt is so much larger than the melt thickness, that we will work in a planar idealisation for the solidification model as shown in Figure 4. The vertical direction is perpendicular to the side wall while the horizontal direction is along the side wall parallel to the axis of the hole.

We now derive the splashing and solidification models in detail for the stages (ii) and (iii) above. We note that these models only describe the situation when the fluid is present. If the fluid is absent, then the standard heat equation is appropriate.

2.2 Solidification model

We consider an incompressible fluid contained in the vertical direction by a bottom defined by $y = \eta(x,t)$ and a top defined by $y = h(x,t)$ as indicated in Figure 4, where x and y are the coordinates in the horizontal (along the side wall) and vertical (perpendicular to the side wall) directions and t is time. Solidified material is present in the region $y < \eta(x,t)$. The initial boundary value problem for the potential $\phi(x,y,t)$, temperature $T(x,y,t)$ and unknown free surfaces $y = \eta(x,t)$ and $y = h(x,t)$ is

$$\nabla^2\phi = 0, \qquad \frac{\partial T}{\partial t} + \boldsymbol{\nabla}\phi\cdot\boldsymbol{\nabla}T = \frac{k}{\rho c}\nabla^2 T \quad \text{for} \quad \eta(x,t) < y < h(x,t), \tag{1}$$

$$\frac{\partial T}{\partial t} = \frac{k}{\rho c}\nabla^2 T \quad \text{for} \quad y < \eta(x,t), \tag{2}$$

$$\frac{D}{Dt}(y-h) = 0, \qquad \frac{\partial\phi}{\partial t} + \frac{1}{2}|\boldsymbol{\nabla}\phi|^2 = 0, \qquad \boldsymbol{\nabla}T\cdot\boldsymbol{\nabla}(y-h) = 0 \quad \text{on} \quad y = h(x,t), \tag{3}$$

$$T = T_m, \qquad \boldsymbol{\nabla}\phi\cdot\boldsymbol{\nabla}(y-\eta) = 0, \qquad \rho L_f\frac{\partial\eta}{\partial t} + [k\boldsymbol{\nabla}T]_{\eta^-}^{\eta^+}\cdot\boldsymbol{\nabla}(y-\eta) = 0 \quad \text{on} \quad y = \eta(x,t), \tag{4}$$

$$T \to T_a \quad \text{as} \quad y \to -\infty, \tag{5}$$

where T_a is the ambient temperature and the differential operator $\boldsymbol{\nabla} = (\partial/\partial x, \partial/\partial y)$. The first boundary condition in (3) is the conservation of mass, the second conservation of momentum and the third conservation of energy. The first boundary condition in (4) is the melting isotherm, the second conservation of mass and the third conservation of energy. The conservation of mass and energy boundary conditions have been derived from the general formulations (see [2]).

We transform to dimensionless variables via $\phi = UL\hat{\phi}$, $T = T_m + (T_v - T_m)\hat{T}$, $\eta = d\hat{\eta}$, $h = d\hat{h}$, $x = L\hat{x}$, $y = d\hat{y}$ and $t = L\hat{t}/U$, where T_v is the vaporisation temperature at one atmosphere pressure. The solidification model then becomes (and without ambiguity the hats on the non-dimensional variables can be omitted)

$$\frac{\partial^2\phi}{\partial x^2} + \frac{1}{\delta^2}\frac{\partial^2\phi}{\partial y^2} = 0, \qquad \frac{\partial T}{\partial t} + \frac{\partial\phi}{\partial x}\frac{\partial T}{\partial x} + \frac{1}{\delta^2}\frac{\partial\phi}{\partial y}\frac{\partial T}{\partial y} = D\left(\delta^2\frac{\partial^2 T}{\partial x^2} + \frac{\partial^2 T}{\partial y^2}\right) \qquad \text{for} \qquad \eta(x,t) < y < h(x,t), \quad (6)$$

$$\frac{\partial T}{\partial t} = D\left(\delta^2\frac{\partial^2 T}{\partial x^2} + \frac{\partial^2 T}{\partial y^2}\right) \qquad \text{for} \qquad y < \eta(x,t), \quad (7)$$

$$\frac{1}{\delta^2}\frac{\partial\phi}{\partial y} = \frac{\partial h}{\partial t} + \frac{\partial\phi}{\partial x}\frac{\partial h}{\partial x}, \qquad \frac{\partial\phi}{\partial t} + \frac{1}{2}\left(\left(\frac{\partial\phi}{\partial x}\right)^2 + \frac{1}{\delta^2}\left(\frac{\partial\phi}{\partial y}\right)^2\right) = 0, \qquad \frac{\partial T}{\partial y} = \delta^2\frac{\partial h}{\partial x}\frac{\partial T}{\partial x} \qquad \text{on} \qquad y = h(x,t), \quad (8)$$

$$T = 0, \qquad \frac{1}{\delta^2}\frac{\partial\phi}{\partial y} = \frac{\partial\phi}{\partial x}\frac{\partial\eta}{\partial x}, \qquad \lambda_f\frac{\partial\eta}{\partial t} + D\left[\frac{\partial T}{\partial y} - \delta^2\frac{\partial\eta}{\partial x}\frac{\partial T}{\partial x}\right]_{\eta^-}^{\eta^+} = 0 \qquad \text{on} \qquad y = \eta(x,t), \quad (9)$$

$$T \to \bar{T}_a \qquad \text{as} \qquad y \to -\infty. \quad (10)$$

The dimensionless constants δ, D, λ_f and $\bar{T}_a$ are defined, and typical values given in Table 2; the constraint $\delta^2 \ll 1$ typically holds in practice. The model is regularly perturbed in this small parameter. The parameter λ_f represents the Stefan number for fusion.

2.3 Splashing model

The same notation for potential, temperature and the moving boundaries will be adopted for the splashing model; these quantities are defined anew. We consider an incompressible fluid contained in the vertical direction by a bottom defined by $z = \eta(r,t)$ and a top defined by $z = h(r,t)$ as indicated in Figure 3, where r and z are the coordinates in the radial and vertical directions and t is time. Solidified material is present in the region $z < \eta(r,t)$. The initial boundary value problem for the potential $\phi(r,z,t)$, temperature $T(r,z,t)$ and unknown free surfaces $z = \eta(r,t)$ and $z = h(r,t)$ is

$$\frac{\partial^2\phi}{\partial r^2} + \frac{1}{r}\frac{\partial\phi}{\partial r} + \frac{\partial^2\phi}{\partial z^2} = 0, \quad \frac{\partial T}{\partial t} + \frac{\partial\phi}{\partial r}\frac{\partial T}{\partial r} + \frac{\partial\phi}{\partial z}\frac{\partial T}{\partial z} = \frac{k}{\rho c}\left\{\frac{\partial^2 T}{\partial r^2} + \frac{1}{r}\frac{\partial T}{\partial r} + \frac{\partial^2 T}{\partial z^2}\right\} \quad \text{for} \quad \eta(r,t) < z < h(r,t), \quad (11)$$

$$\frac{\partial T}{\partial t} = \frac{k}{\rho c}\left\{\frac{\partial^2 T}{\partial r^2} + \frac{1}{r}\frac{\partial T}{\partial r} + \frac{\partial^2 T}{\partial z^2}\right\} \qquad \text{for} \quad z < \eta(r,t), \quad (12)$$

$$T = V, \quad \frac{\partial\phi}{\partial t} + \frac{1}{2}\left(\left(\frac{\partial\phi}{\partial r}\right)^2 + \left(\frac{\partial\phi}{\partial z}\right)^2\right) + \frac{p}{\rho} = 0 \quad \text{on} \quad z = h(r,t), \quad (13)$$

$$-I + k\left(\frac{\partial T}{\partial z} - \frac{\partial h}{\partial r}\frac{\partial T}{\partial r}\right) + \rho L_v\left(-\frac{\partial h}{\partial t} - \frac{\partial h}{\partial r}\frac{\partial\phi}{\partial r} + \frac{\partial\phi}{\partial z}\right) = 0 \quad \text{on} \quad z = h(r,t), \quad (14)$$

$$T = T_m, \quad \frac{\partial\phi}{\partial z} = \frac{\partial\eta}{\partial r}\frac{\partial\phi}{\partial r}, \quad \rho L_f\frac{\partial\eta}{\partial t} + k\left[\frac{\partial T}{\partial z} - \frac{\partial\eta}{\partial r}\frac{\partial T}{\partial r}\right]_{\eta^-}^{\eta^+} = 0 \quad \text{on} \quad z = \eta(r,t), \quad (15)$$

$$T \to T_a \quad \text{as} \quad z \to -\infty, \quad (16)$$

where p is the recoil pressure, I is the input of laser energy, $V(p)$ is the vaporisation temperature as a function of recoil pressure and $L_v(V)$ is the latent heat of vaporisation. The first boundary condition in (13) is the vaporisation isotherm and the second conservation of momentum. Boundary condition (14) represents conservation of energy. The first boundary condition in (15) is the melting isotherm, the second conservation of mass and the third conservation of energy.

The recoil pressure, the input of laser energy and the vaporisation temperature are required to complete the mathematical model for splashing. Ideally these quantities could be obtained from a numerical simulation of the axisymmetric domain above the fluid, but this is computationally expensive. An alternative approach, which involves modelling the domain as an infinite set of one-dimensional problems, is outlined in the Appendix.

We transform to dimensionless variables via $\phi = UL\hat{\phi}$, $T = T_m + (T_v - T_m)\hat{T}$, $\eta = d\hat{\eta}$, $h = d\hat{h}$, $r = L\hat{r}$, $z = d\hat{z}$ and $t = L\hat{t}/U$. The axisymmetric splashing model then becomes (and without ambiguity the hats on the non-dimensional variables can be omitted)

$$\frac{\partial^2\phi}{\partial r^2}+\frac{1}{r}\frac{\partial\phi}{\partial r}+\frac{1}{\delta^2}\frac{\partial^2\phi}{\partial z^2} = 0,\ \ \frac{\partial T}{\partial t}+\frac{\partial\phi}{\partial r}\frac{\partial T}{\partial r}+\frac{1}{\delta^2}\frac{\partial\phi}{\partial z}\frac{\partial T}{\partial z} = D\left\{\delta^2\left(\frac{\partial^2 T}{\partial r^2}+\frac{1}{r}\frac{\partial T}{\partial r}\right)+\frac{\partial^2 T}{\partial z^2}\right\} \text{ for } \eta(r,t) < z < h(r,t), \tag{17}$$

$$\frac{\partial T}{\partial t} = D\left\{\delta^2\left(\frac{\partial^2 T}{\partial r^2}+\frac{1}{r}\frac{\partial T}{\partial r}\right)+\frac{\partial^2 T}{\partial z^2}\right\} \ \text{ for } \ z < \eta(r,t), \tag{18}$$

$$T = \bar{V},\ \frac{\partial\phi}{\partial t}+\frac{1}{2}\left(\frac{\partial\phi}{\partial r}\right)^2+\frac{1}{2\delta^2}\left(\frac{\partial\phi}{\partial z}\right)^2+\bar{p} = 0, \tag{19}$$

$$\frac{1}{\delta^2}\frac{\partial\phi}{\partial z}-\frac{\partial\phi}{\partial r}\frac{\partial h}{\partial r}-\frac{\partial h}{\partial t} = \bar{I}-\frac{D}{\lambda_v\bar{L}_v}\left(\frac{\partial T}{\partial z}-\delta^2\frac{\partial h}{\partial r}\frac{\partial T}{\partial r}\right) \ \text{ on } z = h(r,t), \tag{20}$$

$$T = 0,\ \ \frac{1}{\delta^2}\frac{\partial\phi}{\partial z} = \frac{\partial\phi}{\partial r}\frac{\partial\eta}{\partial r},\ \ \lambda_f\frac{\partial\eta}{\partial t}+D\left[\frac{\partial T}{\partial z}-\delta^2\frac{\partial\eta}{\partial r}\frac{\partial T}{\partial r}\right]_{\eta^-}^{\eta^+} = 0 \ \text{ on } \ z = \eta(r,t), \tag{21}$$

$$T \to \bar{T}_a \quad \text{as} \quad z \to -\infty, \tag{22}$$

where $\bar{V} = (V(p)-T_m)/(T_v-T_m)$, $\bar{p} = p/\rho U^2$, $\bar{I} = IL/\rho dUL_v$ (where typically $\bar{I} \sim 0.1$) and $\bar{L}_v = L_v/L_v(T_v)$ are specified functions. The dimensionless constants δ, D, λ_f, λ_v and $\bar{T}_a$ are defined, and typical values given in Table 2; the constraints $\delta^2 \ll 1$ and $1/\lambda_v \ll 1$ typically hold in practice. The model is regularly perturbed in these small parameters. The parameter λ_v represents the Stefan number for vaporisation.

3 The leading-order problem

3.1 Solidification model

3.1.1 Asymptotic analysis

We now derive the leading-order equations for the solidification model. We introduce expansions of the form

$$\phi \sim \phi_0 + \delta^2\phi_1, \qquad T \sim T_0 + \delta^2 T_1, \qquad h \sim h_0 + \delta^2 h_1, \qquad \eta \sim \eta_0 + \delta^2\eta_1.$$

We transfer the condition from the correct boundary $y = \eta$ to a convenient boundary $y = \eta_0$ by using a Taylor series expansion, that is

$$\left.\frac{\partial\phi}{\partial y}\right|_{y=\eta} = \left.\frac{\partial\phi_0}{\partial y}\right|_{y=\eta_0} + \delta^2\left(\left.\frac{\partial\phi_1}{\partial y}\right|_{y=\eta_0} + \eta_1\left.\frac{\partial^2\phi_0}{\partial y^2}\right|_{y=\eta_0}\right) + O(\delta^4).$$

A similar transfer takes place between $y = h$ and $y = h_0$. From the first equation in (6) and the second boundary condition in (9) we obtain

$$\phi \sim a + \delta^2\left\{b - \frac{a_{xx}y^2}{2} + (a_x\eta_0)_x y\right\} \tag{23}$$

where $a = a(x,t)$ and $b = b(x,t)$ are unknown functions. Substituting (23) into the second equation in (6), the first boundary condition in (8) and the second boundary condition in (8) gives

$$\frac{\partial T_0}{\partial t} + a_x \frac{\partial T_0}{\partial x} + \{(a_x \eta_0)_x - a_{xx} y\} \frac{\partial T_0}{\partial y} = D \frac{\partial^2 T_0}{\partial y^2}, \qquad \frac{\partial h_0}{\partial t} + \frac{\partial}{\partial x}\{a_x (h_0 - \eta_0)\} = 0, \qquad a_t + \frac{(a_x)^2}{2} = 0,$$

respectively. Finally, we make the substitution $u = a_x$ to give a differential equation for the temperature:

$$\frac{\partial T_0}{\partial t} + u \frac{\partial T_0}{\partial x} + \{(u\eta_0)_x - u_x y\} \frac{\partial T_0}{\partial y} = D \frac{\partial^2 T_0}{\partial y^2} \qquad \text{for} \qquad \eta_0 < y < h_0, \tag{24}$$

with two boundary conditions:

$$\text{on} \qquad y = \eta_0, \qquad T_0 = 0; \qquad \text{on} \qquad y = h_0, \qquad \frac{\partial T_0}{\partial y} = 0. \tag{25}$$

The equation for the evolution of the velocity is

$$u_t + u u_x = 0, \tag{26}$$

and the equations for the evolution of the free boundaries are

$$\frac{\partial h_0}{\partial t} + \frac{\partial}{\partial x}\{u(h_0 - \eta_0)\} = 0, \qquad \lambda_f \frac{\partial \eta_0}{\partial t} + D \left[\frac{\partial T_0}{\partial y} \right]_{\eta_0^-}^{\eta_0^+} = 0, \tag{27}$$

while the equation and the boundary condition for conduction in the solid are

$$\frac{\partial T_0}{\partial t} = D \frac{\partial^2 T_0}{\partial y^2} \qquad \text{for} \qquad y < \eta_0 \qquad \text{and} \qquad T_0 \to \bar{T}_a \qquad \text{as} \qquad y \to -\infty. \tag{28}$$

The leading-order equations to describe solidification are (24)–(28). These equations are a combination of the shallow water equations in the zero gravity limit and a two-phase Stefan problem. The appearance of the thermal convection in the vertical direction in the leading-order equations is due to the large vertical thermal gradients balancing with small vertical velocities. We note that this model only has a three-dimensional parameter space.

3.1.2 Shocks

We note that (26) uncouples from the system of equations (24)–(28). Let $u(x,0) = \tilde{u}(x)$ describe the initial velocity distribution; then $u(x,t)$ is given implicitly by $u = \tilde{u}(x - ut)$. Moreover, the slope is given by

$$u_x = \frac{\tilde{u}'(X)}{1 + t\tilde{u}'(X)}, \qquad X = x - ut.$$

We have the following cases (i) $\tilde{u}'(X) \geq 0$ for all X so that no shocks develop or (ii) a shock will develop after a time given by $-1/\tilde{u}'(X_s)$ where X_s is the value of steepest negative slope. Case (ii) occurs in practice because the melt will always have compact support.

In the case of shocks it is necessary to obtain Rankine-Hugoniot conditions for the full system of equations. We need to rewrite (24), (26) and the first equation in (27) in conservation form

$$\frac{\partial}{\partial t}(h_0 - \eta_0) + \frac{\partial}{\partial x}(u(h_0 - \eta_0)) = -\frac{\partial \eta_0}{\partial t}, \tag{29}$$

$$\frac{\partial}{\partial t}(u(h_0 - \eta_0)) + \frac{\partial}{\partial x}(u^2(h_0 - \eta_0)) = -u\frac{\partial \eta_0}{\partial t}, \tag{30}$$

$$\frac{\partial T_0}{\partial t} + \frac{\partial}{\partial x}(uT_0) + \frac{\partial}{\partial y}\left(\{(u\eta_0)_x - u_x y\}\, T_0 - D\frac{\partial T_0}{\partial y}\right) = 0. \tag{31}$$

Equation (29) is conservation of mass, (30) is conservation of momentum and (31) is conservation of energy. We neglect kinetic energy in (31) because $U^2/cT_m \ll 1$. The corresponding Rankine-Hugoniot conditions are $[h_0 - \eta_0]Q = [u(h_0 - \eta_0)]$, $[u(h_0 - \eta_0)]Q = [u^2(h_0 - \eta_0)]$ and $[T_0]Q = [uT_0]$ where square brackets denote the difference between the values of the quantity on the two sides of the shock and Q is the speed of the shock. The Rankine-Hugoniot condition for conservation of energy represents an infinite set of conditions parameterised by y.

The leading edge of the melt (of finite extent) will always be a shock. However, there is no mass flux through this leading-edge shock. The accumulation of solidified material (recast) is considered to be related to shocks behind which melt can amass.

3.1.3 Summary of the leading-order solidification problem

The conservative form of the equations in the fluid (29)–(31) indicate that a more natural choice of dependent variable is the film thickness $H = h_0 - \eta_0$ rather than h_0. We also replace T_0 and η_0 by θ and ψ to avoid complications with subscripts in subsequent asymptotic expansions. A simpler form of the system of equations suitable for numerical solution is given by

$$\frac{\partial H}{\partial t} + \frac{\partial}{\partial x}(uH) = -\frac{\partial \psi}{\partial t}, \qquad \frac{\partial}{\partial t}(uH) + \frac{\partial}{\partial x}(u^2 H) = -u\frac{\partial \psi}{\partial t}, \tag{32}$$

$$\frac{\partial \theta}{\partial t} + \frac{\partial}{\partial x}(u\theta) + \frac{\partial}{\partial y}\left(\{(u\psi)_x - u_x y\}\,\theta - D\frac{\partial \theta}{\partial y}\right) = 0, \quad \text{with} \quad \frac{\partial \theta}{\partial y} = 0 \quad \text{on} \quad y = \psi + H \quad , \tag{33}$$

for the fluid velocity and temperature, with the interface condition

$$\lambda_f \frac{\partial \psi}{\partial t} + D\left[\frac{\partial \theta}{\partial y}\right]_{\psi^-}^{\psi^+} = 0, \quad \text{on} \quad y = \psi \quad \theta = 0, \tag{34}$$

and

$$\frac{\partial \theta}{\partial t} = D\frac{\partial^2 \theta}{\partial y^2} \quad \text{for} \quad y < \psi \quad \text{and} \quad \theta \to \bar{T}_a \quad \text{as} \quad y \to -\infty, \tag{35}$$

in the solid. The initial conditions are

$$u(x,0) = \tilde{u}(x), \qquad \theta(x,y,0) = \tilde{\theta}(x,y), \qquad H(x,0) = \tilde{H}(x), \qquad \psi(x,0) = 0. \tag{36}$$

where we assume $\tilde{\theta}(x,y) = \bar{T}_a$ for $y < 0$, and $\tilde{\theta}(x,0) = 0$ and $\partial\tilde{\theta}/\partial y(x, \tilde{H}(x)) = 0$ for $\tilde{H}(x) > 0$. The Rankine-Hugoniot conditions are given by

$$[H]Q = [uH], \qquad [uH]Q = [u^2 H], \qquad [\theta]Q = [u\theta]. \tag{37}$$

We note that the right-hand side of the equation for conservation of mass is the rate at which the material is solidified. Similar comments apply to the equation for conservation of momentum. Equations (32) are valid for plug flow independent of the irrotational assumptions which were required to construct the model in Subsection 2.2. The only term in which the form of the potential remains is the vertical convection of energy in (33); this term being essential to guarantee the appropriate enthalpy flux at $y = \psi$ and $y = \psi + H$. The initial temperature of the solid is assumed to be ambient in the cold side wall of the drilled hole. The initial temperature of the fluid is at melting point at the fluid/solid interface; there being a discontinuous spatial derivative at $y = 0$ in the initial temperature.

3.2 Splashing model

We now summarise the splashing model in conservation form. We define the leading-order quantity $u(r,t)$ to be the radial velocity, $\theta(r,z,t)$ the temperature, $\psi(r,t)$ the position of the fluid/solid boundary and $H(r,t)$ the film thickness. We obtain equations for conservation of mass, momentum and energy

$$\frac{\partial H}{\partial t}+\frac{1}{r}\frac{\partial}{\partial r}(ruH)=-\left(\bar{I}+\frac{\partial\psi}{\partial t}\right),\qquad \frac{\partial}{\partial t}(uH)+\frac{1}{r}\frac{\partial}{\partial r}(ru^2H)=-u\left(\bar{I}+\frac{\partial\psi}{\partial t}\right)-H\frac{\partial\bar{p}}{\partial r}, \tag{38}$$

$$\frac{\partial\theta}{\partial t}+\frac{1}{r}\frac{\partial}{\partial r}(ru\theta)+\frac{\partial}{\partial z}\left(\left\{\frac{1}{r}\frac{\partial}{\partial r}(ru\psi)-\frac{z}{r}\frac{\partial}{\partial r}(ru)\right\}\theta-D\frac{\partial\theta}{\partial z}\right)=0,\qquad \text{with}\quad \theta=\bar{V}\quad \text{on}\quad z=\psi+H, \tag{39}$$

in the fluid, the Stefan condition and melting isotherm

$$\lambda_f\frac{\partial\psi}{\partial t}+D\left[\frac{\partial\theta}{\partial z}\right]_{\psi^-}^{\psi^+}=0,\qquad \text{with}\quad \theta=0\quad \text{on}\quad z=\psi, \tag{40}$$

at the interface and the heat equation and far-field condition

$$\frac{\partial\theta}{\partial t}=D\frac{\partial^2\theta}{\partial z^2}\quad \text{for}\quad z<\psi\quad \text{and}\quad \theta\to\bar{T}_a\quad \text{as}\quad z\to-\infty, \tag{41}$$

in the solid. The initial conditions are

$$u(r,0)=0,\qquad \theta(r,z,0)=\tilde{\theta}(r,z),\qquad H(r,0)=\tilde{H}(r),\qquad \psi(r,0)=0. \tag{42}$$

where we assume $\tilde{\theta}\to\bar{T}_a$ as $z\to-\infty$, and $\tilde{\theta}(r,0)=0$ and $\tilde{\theta}(r,\tilde{H})=\bar{V}$ for $\tilde{H}(r)>0$. The Rankine-Hugoniot conditions are identical to those for the solidification problem. We note that the first term on the right-hand side of the equation for conservation of mass represents evaporation and the second solidification. These effects are both present on the right-hand side of the conservation of momentum equation along with the radial pressure gradient term. Equations (38) are valid for plug flow independent of the irrotational assumptions. The previous comments concerning (33) may now be applied to (39). The initial temperature in the splashing model corresponds to the final time in melt-pool formation (see Figure 1) when the liquid/gas interface reaches vaporisation temperature.

4 Analytical solution of the solidification problem

4.1 The large-time limit: similarity transformation

We now consider self-similar solutions which may occur whilst drilling deep holes ($\sim$ 10mm); this being motivated by a continuous symmetry group of (24)–(28). It is difficult, and rare in practice, to prove that self-similar solutions, independent of the detailed structure of the initial conditions, develop in the large-time limit of a system of partial differential equations. In general, numerical techniques are required to determine whether a self-similar solution is approached at large times. However, equation (26) uncouples so that it is possible to show that $u_x\sim 1/t$ and $u_t\sim -u/t$ for $t\gg 1$, $x/t=O(1)$ and $\tilde{u}'(X)>0$. We will assume the initial velocity distribution is such that there are no shocks apart from at the leading edge, that is $\tilde{u}'(X)\geq 0$. Therefore,

$$u\sim\begin{cases} x/t & \tilde{u}'(X)>0,\\ \tilde{u} & \tilde{u}'(X)=0,\end{cases}$$

for $t\gg 1$ and $x/t=O(1)$. This demonstrates that the large-time solution for the velocity is self-similar and independent of the detailed structure of the initial velocity at leading order. The thermal energy is initially localised in the molten metal. We are interested in time-scales such that the conduction length-scale is much

larger than the vertical dimension of the fluid drop. Therefore the detailed structure of the initial condition will have smoothed under the action of conduction. The initial condition for the solidification boundary has no detailed structure. The molten drop is assumed to have spread to a length-scale significantly greater than the initial support of the drop $x \in [0, X_U(t)]$, where $X_U(t)$ is the leading-edge shock. We will seek a solution in an expanding domain with zero mass, momentum and energy flux boundary conditions at $x = 0$. The fluid layer is assumed to be deep enough that solidification does not engulf the flow at any point during this intermediate time stage. This idealisation will provide valuable physical insight.

Based on the above assumptions, the solidification problem has a similarity solution with

$$T_0 = \bar{T}(\zeta, \xi), \quad u = \bar{u}(\zeta), \quad \eta_0 = t^{1/2}\bar{\eta}(\zeta), \quad h_0 = t^{1/2}\bar{h}(\zeta)$$

where $\zeta = x/t$ and $\xi = y/\sqrt{t}$. The similarity variable ζ is characteristic of inertia (it being common in solutions of the shallow water equations) and the similarity variable ξ is characteristic of solidification (it being common in solutions of one-dimensional Stefan problems). Equations (24)–(28) transform to

$$(\bar{u} - \zeta)\frac{\partial \bar{T}}{\partial \zeta} + \left\{ \frac{\mathrm{d}(\bar{u}\bar{\eta})}{\mathrm{d}\zeta} - \xi\left(\frac{1}{2} + \frac{\mathrm{d}\bar{u}}{\mathrm{d}\zeta}\right)\right\}\frac{\partial \bar{T}}{\partial \xi} = D\frac{\partial^2 \bar{T}}{\partial \xi^2} \quad \text{for} \quad \bar{\eta} < \xi < \bar{h}, \tag{43}$$

$$-\zeta\frac{\partial \bar{T}}{\partial \zeta} - \frac{\xi}{2}\frac{\partial \bar{T}}{\partial \xi} = D\frac{\partial^2 \bar{T}}{\partial \xi^2} \quad \text{for} \quad \xi < \bar{\eta}, \tag{44}$$

$$(\bar{u} - \zeta)\frac{\mathrm{d}\bar{u}}{\mathrm{d}\zeta} = 0, \quad \frac{\bar{h}}{2} - \zeta\frac{\mathrm{d}\bar{h}}{\mathrm{d}\zeta} + \frac{\mathrm{d}(\bar{u}\bar{h})}{\mathrm{d}\zeta} = \frac{\mathrm{d}(\bar{u}\bar{\eta})}{\mathrm{d}\zeta}, \quad \lambda_f\left(\frac{\bar{\eta}}{2} - \zeta\frac{\mathrm{d}\bar{\eta}}{\mathrm{d}\zeta}\right) + D\left[\frac{\partial \bar{T}}{\partial \xi}\right]_{\xi=\bar{\eta}^-}^{\xi=\bar{\eta}^+} = 0, \tag{45}$$

$$\bar{T} = 0 \quad \text{on} \quad \xi = \bar{\eta}, \quad \frac{\partial \bar{T}}{\partial \xi} = 0 \quad \text{on} \quad \xi = \bar{h}, \quad \bar{T} \to \bar{T}_a \quad \text{as} \quad \xi \to -\infty. \tag{46}$$

for $0 < \zeta < \zeta_U$ where the constant $\zeta_U = X_U/t$. In the absence of shocks, other than the leading-edge shock, the resolidification will be in the form of thin layers.

The first equation in (45) implies that either $\bar{u} = \zeta$, $\bar{u}$ is a constant or a combination of these. The choice adopted depends on the initial velocity distribution ($u(x, 0) = \tilde{u}(x)$). If we select $\tilde{u}(0) = 0$ and $\tilde{u}'(x) > 0$ where $\bar{h} > \bar{\eta}$, then the large-time velocity will be of the form $\bar{u} \sim \zeta$, that is $u \sim x/t$. The zero mass, momentum and energy flux boundary conditions at $\zeta = 0$ are automatically satisfied as $\bar{u}(0) = 0$. The Rankine-Hugoniot conditions (37) are satisfied with $Q = \zeta_U$ at the leading-edge shock. We may now solve (43) subject to the first and second boundary conditions in (46) to obtain $\bar{T} = 0$ for $\bar{\eta} < \xi < \bar{h}$; the liquid is then at the melting point. The system of equations reduces to (44) with the first and third boundary conditions in (46) along with

$$\frac{3\bar{h}}{2} = \frac{\mathrm{d}(\zeta\bar{\eta})}{\mathrm{d}\zeta}, \quad \lambda_f\left(\frac{\bar{\eta}}{2} - \zeta\frac{\mathrm{d}\bar{\eta}}{\mathrm{d}\zeta}\right) = D\left.\frac{\partial \bar{T}}{\partial \xi}\right|_{\xi=\bar{\eta}^-}. \tag{47}$$

The first equation in (47) uncouples and we do not consider it any further. Therefore, the resolidified boundary is independent of the fluid depth in this case. We make the transformation to the new independent variables $s = \xi - \bar{\eta}(\zeta)$ and $q = \ln(1/\zeta)$ to obtain

$$\frac{\partial \bar{T}}{\partial q} - \frac{\partial \bar{T}}{\partial s}\left(\frac{s}{2} + \frac{D}{\lambda_f}\left.\frac{\partial \bar{T}}{\partial s}\right|_{s=0^-}\right) = D\frac{\partial^2 \bar{T}}{\partial s^2}, \tag{48}$$

subject to the boundary conditions

$$\text{on} \quad s = 0 \quad \bar{T} = 0, \quad \bar{T} \to \bar{T}_a \quad \text{as} \quad s \to -\infty, \tag{49}$$

and the initial condition $\bar{T}(s, 0) = w(s)$, where $w(s)$ may only be determined numerically. Equation (48) is a nonlinear convection-diffusion equation.

4.2 Small diffusion

In this subsection we assume that $D \ll 1$ and a particular $\tilde{u}(x)$ which allows us to make analytical progress with the system of equations (32)–(36); the choice of initial velocity distribution being given by $\tilde{u}(x) = x$ for $0 \leq x \leq 1$ and $\tilde{u}(x) = 0$ otherwise. The model is singularly perturbed in the small parameter D. Small diffusion corresponds to the molten metal having a high velocity after the splash. The results in this section may be used to validate a numerical solution.

We introduce expansions of the form $u \sim u_0$, $\theta \sim \theta_0$, $H \sim H_0$ and $\psi \sim D^{1/2}\psi_0$. The following solutions are obtained in the fluid:

$$u_0 = \frac{x}{1+t}, \qquad \theta_0 = \tilde{\theta}\left(\frac{x}{1+t}\ ,\ y(1+t)\right), \qquad H_0 = \frac{1}{1+t}\tilde{H}\left(\frac{x}{1+t}\right) \quad \text{for} \quad 0 \leq x \leq 1+t.$$

We note that θ_0 satisfies both the boundary conditions given by the second equation in (33) and the second equation in (34). Therefore there is no boundary layer in the fluid despite the removal of the highest derivative in the leading-order problem. In the solid there is an outer expansion and an inner expansion near $y = \psi$. The outer expansion is given by $\theta \sim \bar{T}_a$. We perform the stretching transformation $y = D^{1/2}Y$ in the boundary layer, to obtain the leading-order problem

$$\frac{\partial \theta_0}{\partial t} = \frac{\partial^2 \theta_0}{\partial Y^2}, \quad \theta_0(x, \psi_0, t) = 0 \text{ for } t > t^*, \quad \theta_0 \to \bar{T}_a \text{ as } Y \to -\infty, \quad \theta_0(x, Y, t^*) = \bar{T}_a, \quad \lambda_f \frac{\partial \psi_0}{\partial t} = \left.\frac{\partial \theta_0}{\partial Y}\right|_{Y=\psi_0^-}$$

where $t^* = \max(x-1, 0)$. We thus have

$$\theta_0 = \bar{T}_a - \frac{\bar{T}_a}{1 + \operatorname{erf}(\bar{\psi}/2)}\left(1 + \operatorname{erf}\left(\frac{Y}{2\sqrt{t - \max(x-1,0)}}\right)\right) \quad \text{for} \quad t \geq \max(x-1, 0),$$

where $\bar{\psi}$ is the unique root of the transcendental equation

$$\lambda_f \sqrt{\pi}\bar{\psi} \exp\left(\frac{\bar{\psi}^2}{4}\right)\left(1 + \operatorname{erf}\left(\frac{\bar{\psi}}{2}\right)\right) = -2\bar{T}_a,$$

provided that $\bar{T}_a < \lambda_f$. Finally, $\psi_0 = \bar{\psi}\sqrt{t - \max(x-1, 0)}$. This is essentially the Neumann solution [15, p. 158]. The temperature in the fluid does not influence the leading-order term for solidification due to the absence of large temperature gradients.

The solution for $t = O(1)$ is an inner solution which breaks down on the longer time-scale $t = O(D^{-1/3})$. A number of variables need to be rescaled in this outer region, that is $t = D^{-1/3}\bar{t}$, $x = D^{-1/3}\bar{x}$, $y = D^{1/3}\bar{y}$, $H = D^{1/3}\bar{H}$ and $\psi = D^{1/3}\bar{\psi}$. The leading-order problem on this longer time-scale corresponds to a complete balance and no further analytical progress is possible. We note that for deep holes and small diffusion, the thickness of the resolidified material is $O(D^{1/3})$ spread over a region $O(D^{-1/3})$.

The time derivative of the solidified boundary ψ becomes infinite as $t \to t^*$ and it appears that this motivates a further inner layer in time due to the right-hand side of equations (32) entering the leading-order balance. However, it should be recalled that these equations are derived from (26) and $(27)_1$ by subtracting the singular term from both sides of the equation. Therefore no further inner layer is required.

5 Weak formulation

5.1 Introduction

Weak formulations have been studied widely in the context of the Stefan problem (see [3] and references therein). However, the Stefan problem in which the fluid is moving across a solid surface has received scant

attention. The purpose of this section is to incorporate a weak formulation of the conservation of energy equation into our models for solidification and splashing. Moreover, we prove that solutions of the weak formulations include all classical solutions. The novelty of this approach is that the Enthalpy method is formulated on a moving domain which follows the location of the fluid with the advantage that only a section of the domain requires meshing at any given time.

5.2 Solidification problem

We define $X_L(t)$ and $X_U(t)$ to be the points $X_L(t) = \inf\{x : H(x,t) > 0\}$ and $X_U(t) = \sup\{x : H(x,t) > 0\}$ (shown in Figure 4). We assume that the fluxes of mass, momentum and energy are zero at the limits of the fluid region, so that

$$uH = u^2H = u\theta = 0 \quad \text{on } x = X_L(t)^-, X_U(t)^+ \text{ and } y = \psi. \tag{50}$$

If $u \geq 0$ then (50) on $x = X_L(t)^-$ are boundary conditions for (32)–(33); the case $u \leq 0$ being similar. Let $\Omega(t)$ be the region in $\mathbb{R}^2$ such that $X_L(t) < x < X_U(t)$ and $y < \psi + H$. For any $\tau > 0$, let $\Omega_\tau = \bigcup_{t<\tau} \Omega(t)$. We define

$$\begin{aligned} \Omega^+(t) &= \{(x,y) \in \Omega(t) : S(x,y,t) > 0 \text{ and } \theta > 0\} \text{ (liquid)}, \\ \Omega^-(t) &= \{(x,y) \in \Omega(t) : S(x,y,t) < 0 \text{ and } \theta < 0\} \text{ (solid)}, \end{aligned}$$

$$\Gamma = \{(x,y,t) \in \Omega_\tau : S(x,y,t) = 0\}, \;\; \Omega_\tau^+ = \bigcup_{t<\tau} \Omega^+(t), \;\; \Omega_\tau^- = \bigcup_{t<\tau} \Omega^-(t),$$

where $S(x,y,t) = y - \psi(x,t)$. We define the dimensionless enthalpy, E, by

$$E = \begin{cases} \theta & \theta < 0 \quad \text{(solid)}, \\ \theta + \lambda_f & \theta > 0 \quad \text{(liquid)}, \end{cases}$$

and therefore

$$\theta = \begin{cases} E & E < 0, \\ 0 & 0 < E < \lambda_f, \\ E - \lambda_f & E > \lambda_f. \end{cases} \tag{51}$$

The classical formulation of $(33)_1$ and $(35)_1$ may be written in the form

$$\frac{\partial E}{\partial t} + \frac{\partial}{\partial x}(\chi u\theta) + \frac{\partial}{\partial y}\left(\chi\left\{\frac{\partial}{\partial x}(u\psi) - \frac{\partial u}{\partial x}y\right\}\theta - D\frac{\partial \theta}{\partial y}\right) = 0 \text{ for } (x,y,t) \in \Omega_\tau \setminus \Gamma, \tag{52}$$

where χ is the Heaviside function

$$\chi = \begin{cases} 0 & \theta < 0 \quad \text{(solid)}, \\ 1 & \theta > 0 \quad \text{(liquid)}. \end{cases}$$

We define the functions $\{\theta,\ S\}$ to be a classical solution if

(A) θ, $\partial S/\partial t$ and $\boldsymbol{\nabla} S$ are continuous on Ω_τ,

(B) $\partial\theta/\partial t$, $\boldsymbol{\nabla}\theta$ and $\nabla^2\theta$ are continuous on $\Omega_\tau \setminus \Gamma$,

(C) (32), $(33)_2$, (34), $(35)_2$, (36), (50), (51) and (52) are satisfied.

We define a weak solution of the solidification model to be a pair of bounded integrable functions $\{\theta,\ E\}$ defined on Ω_τ such that (32), $(35)_2$, (36), (50) and (51) are satisfied and the integral identity

$$\int_{\Omega_\tau}\left(E\frac{\partial v}{\partial t} + \chi u\theta\frac{\partial v}{\partial x} + \chi\left\{\frac{\partial}{\partial x}(u\psi) - \frac{\partial u}{\partial x}y\right\}\theta\frac{\partial v}{\partial y} + D\theta\frac{\partial^2 v}{\partial y^2}\right)dydxdt$$

$$= -\int_{\Omega(0)} v(x,y,0)E(x,y,0)dydx + \int_{t=0}^{\tau}\int_{x=X_L(t)}^{X_U(t)} v(x,\psi+H,t)\lambda_f \frac{\partial}{\partial x}(uH)dxdt$$
$$+\int_{t=0}^{\tau}\int_{y=-\infty}^{\psi(X_L(t),t)} \frac{\mathrm{d}X_L}{\mathrm{d}t} v(X_L(t),y,t)\theta(X_L(t),y,t)dydt - \int_{t=0}^{\tau}\int_{y=-\infty}^{\psi(X_U(t),t)} \frac{\mathrm{d}X_U}{\mathrm{d}t} v(X_U(t),y,t)\theta(X_L(t),y,t)dydt \tag{53}$$

holds for all test functions $v \in \mathcal{F}$, where

$$\mathcal{F} = \left\{ \phi \in C^1(\bar{\Omega}_\tau) : \frac{\partial^2 \phi}{\partial x_i \partial x_j} \in C(\bar{\Omega}_\tau),\ \phi(x,y,\tau) = 0,\ \frac{\partial \phi}{\partial y}(x,\psi+H,t) = 0,\ \phi \to 0 \text{ as } y \to -\infty \right\}.$$

If θ were to be replaced by E in the convection terms in (52), that is

$$\frac{\partial E}{\partial t} + \frac{\partial}{\partial x}(\chi u E) + \frac{\partial}{\partial y}\left(\chi \left\{ \frac{\partial}{\partial x}(u\psi) - \frac{\partial u}{\partial x} y \right\} E - D\frac{\partial \theta}{\partial y}\right) = 0 \ \text{ for } (x,y,t) \in \Omega_\tau \setminus \Gamma,$$

then the second term on the right-hand side of (53) would be removed. The formulation (52) is preferred because $\theta(x,\psi,t) = 0$ and θ is continuous whereas the enthalpy E is discontinuous at $y = \psi$ which may well increase discretisation errors. The most important implication of the weak formulation is that the discretisation of (32), $(33)_2$, $(35)_2$, (36), (50), (51) and (52) may converge to a weak solution as the mesh size tends to zero (a proof exists for the standard Stefan problem, see [3] and references therein). Further investigation of these conjectures is required along with the questions of existence, uniqueness and well-posedness.

Theorem 1

1. A classical solution is also a weak solution.
2. If $\{\theta,\ E\}$ is a weak solution and there is a function S such that (34), (A) and (B) hold, then $\{\theta,\ S\}$ is a classical solution.

Proof

1. Let $v \in \mathcal{F}$. If $\{\theta,\ S\}$ is a classical solution then

$$\begin{aligned} 0 &= \int_{\Omega_\tau^+} v\left(\frac{\partial E}{\partial t} + \frac{\partial}{\partial x}(\chi u\theta) + \frac{\partial}{\partial y}\left(\chi\left\{\frac{\partial}{\partial x}(u\psi) - \frac{\partial u}{\partial x}y\right\}\theta - D\frac{\partial\theta}{\partial y}\right)\right)dydxdt \\ &= -\int_{\Omega_\tau^+}\left(E\frac{\partial v}{\partial t} + \chi u\theta\frac{\partial v}{\partial x} + \chi\left\{\frac{\partial}{\partial x}(u\psi) - \frac{\partial u}{\partial x}y\right\}\theta\frac{\partial v}{\partial y} + D\theta\frac{\partial^2 v}{\partial y^2}\right)dydxdt \\ &\quad + \int_{\Omega_\tau^+}\frac{\partial}{\partial t}(vE) + \frac{\partial}{\partial x}(v\chi u\theta) + \frac{\partial}{\partial y}\left(v\chi\left\{\frac{\partial}{\partial x}(u\psi) - \frac{\partial u}{\partial x}y\right\}\theta - Dv\frac{\partial\theta}{\partial y} + D\theta\frac{\partial v}{\partial y}\right)dydxdt. \end{aligned}$$

Now, by the divergence theorem,

$$\begin{aligned} &\int_{\Omega_\tau^+}\left(E\frac{\partial v}{\partial t} + \chi u\theta\frac{\partial v}{\partial x} + \chi\left\{\frac{\partial}{\partial x}(u\psi) - \frac{\partial u}{\partial x}y\right\}\theta\frac{\partial v}{\partial y} + D\theta\frac{\partial^2 v}{\partial y^2}\right)dydxdt \\ &= \int_{\partial\Omega_\tau^+}\left(vE,\ v\chi u\theta,\ v\chi\left\{\frac{\partial}{\partial x}(u\psi) - \frac{\partial u}{\partial x}y\right\}\theta - Dv\frac{\partial\theta}{\partial y} + D\theta\frac{\partial v}{\partial y}\right)\cdot(n_t,\ n_x,\ n_y)dS \\ &= -\int_{\Omega^+(0)} v(x,y,0)E(x,y,0)dydx + \int_{t=0}^{\tau}\int_{x=X_L(t)}^{X_U(t)} v(x,\psi+H,t)\lambda_f\frac{\partial}{\partial x}(uH)dxdt \\ &\qquad + \int_\Gamma v\left(E\frac{\partial\psi}{\partial t} + D\frac{\partial\theta}{\partial y}\right)\frac{dS}{|n|}, \end{aligned} \tag{54}$$

where $|n|^2 = (\partial\psi/\partial t)^2 + (\partial\psi/\partial x)^2 + 1$. We have used the final condition on v, the boundary conditions for $\partial\psi/\partial y$ and $\partial v/\partial y$ on $y = \psi + H$ and the boundary conditions for θ on $y = \psi$. Similarly for Ω_τ^-, we obtain

$$\begin{aligned}
&\int_{\Omega_\tau^-} \left(E\frac{\partial v}{\partial t} + \chi u\theta\frac{\partial v}{\partial x} + \chi\left\{\frac{\partial}{\partial x}(u\psi) - \frac{\partial u}{\partial x}y\right\}\theta\frac{\partial v}{\partial y} + D\theta\frac{\partial^2 v}{\partial y^2}\right) dydxdt \\
&= -\int_{\Omega^-(0)} v(x,y,0)E(x,y,0)dydx - \int_\Gamma v\left(E\frac{\partial\psi}{\partial t} + D\frac{\partial\theta}{\partial y}\right)\frac{dS}{|n|} \\
&+ \int_{t=0}^{\tau}\int_{y=-\infty}^{\psi(X_L(t),t)} \frac{\mathrm{d}X_L}{\mathrm{d}t} v(X_L(t),y,t)\theta(X_L(t),y,t)dydt \\
&- \int_{t=0}^{\tau}\int_{y=-\infty}^{\psi(X_U(t),t)} \frac{\mathrm{d}X_U}{\mathrm{d}t} v(X_U(t),y,t)\theta(X_L(t),y,t)dydt. \qquad (55)
\end{aligned}$$

The third term on the right-hand side of (54) and the second term on the right-hand side of (55) cancel due to $(34)_1$, therefore the classical solution satisfies (53).

2. Let $v \in C_0^\infty(\Omega_\tau^+)$. Then, substituting into (53),

$$\begin{aligned}
0 &= \int_{\Omega_\tau^+} \left(E\frac{\partial v}{\partial t} + \chi u\theta\frac{\partial v}{\partial x} + \chi\left\{\frac{\partial}{\partial x}(u\psi) - \frac{\partial u}{\partial x}y\right\}\theta\frac{\partial v}{\partial y} + D\theta\frac{\partial^2 v}{\partial y^2}\right) dydxdt \\
&= -\int_{\Omega_\tau^+} v\left(\frac{\partial E}{\partial t} + \frac{\partial}{\partial x}(\chi u\theta) + \frac{\partial}{\partial y}\left(\chi\left\{\frac{\partial}{\partial x}(u\psi) - \frac{\partial u}{\partial x}y\right\}\theta - D\frac{\partial\theta}{\partial y}\right)\right) dydxdt.
\end{aligned}$$

Since θ is smooth, we have (52) in Ω_τ^+ and the same argument holds for Ω_τ^-. The boundary condition $(33)_2$ and Stefan condition $(34)_1$ are obtained by taking test functions whose supports are neighbourhoods of the surfaces $y - \psi - H = 0$ and Γ, respectively.

5.3 Splashing problem

We define $R_U(t)$ to be $R_U(t) = \sup\{r : H(r,t) > 0\}$ (shown in Figure 3). We assume that the fluxes of mass, momentum and energy are zero at the limit of the fluid region, so that

$$\text{on } \ r = R_U(t)^+ \ \text{ and } \ z = \psi \qquad uH = u^2H = u\theta = 0. \qquad (56)$$

Let $\Omega(t)$ be the region in $\mathbb{R}^2$ such that $0 < r < R_U(t)$ and $z < \psi + H$. For any $\tau > 0$, let $\Omega_\tau = \bigcup_{t<\tau}\Omega(t)$. We again define $\Gamma = \{(r,z,t) \in \Omega_\tau : S(r,z,t) = 0\}$ where $S(r,z,t) = z - \psi(r,t)$. The classical formulation of $(39)_1$ and $(41)_1$ may be written in the form

$$\frac{\partial E}{\partial t} + \frac{1}{r}\frac{\partial}{\partial r}(\chi r u\theta) + \frac{\partial}{\partial z}\left(\chi\left\{\frac{1}{r}\frac{\partial}{\partial r}(ru\psi) - \frac{z}{r}\frac{\partial}{\partial r}(ru)\right\}\theta - D\frac{\partial\theta}{\partial z}\right) = 0 \ \text{ for } (r,z,t) \in \Omega_\tau \setminus \Gamma. \qquad (57)$$

We define the functions $\{\theta,\ S\}$ to be a classical solution if (A) and (B) hold and

(D) (38), $(39)_2$, (40), $(41)_2$, (42), (51), (56) and (57) are satisfied.

We now define a weak solution of the splashing model to be a pair of bounded integrable functions $\{\theta,\ E\}$ defined on Ω_τ such that (38), $(41)_2$, (42), (51) and (56) are satisfied and the integral identity

$$\begin{aligned}
&\int_{\Omega_\tau} E\frac{\partial v}{\partial t} + \chi u\theta\frac{\partial v}{\partial r} + \chi\left\{\frac{1}{r}\frac{\partial}{\partial r}(ru\psi) - \frac{z}{r}\frac{\partial}{\partial r}(ru)\right\}\theta\frac{\partial v}{\partial z} + D\theta\frac{\partial^2 v}{\partial z^2} r dtdrdz \\
&= -\int_{\Omega(0)} v(r,z,0)E(r,z,0)rdrdz + \int_{t=0}^{\tau}\int_{r=0}^{R_U(t)} \frac{\partial v}{\partial z}(r,\psi+H,t)D\bar{V}rdrdt
\end{aligned}$$

$$-\int_{t=0}^{\tau}\int_{z=-\infty}^{\psi(R_U(t),t)}\frac{\mathrm{d}R_U}{\mathrm{d}t}v(R_U(t),z,t)\theta(R_U(t),z,t)dzdt-\int_{t=0}^{\tau}\int_{z=\psi(0,t)}^{\psi(0,t)+H(0,t)}u(0,t)v(0,z,t)\theta(0,z,t)dzdt \quad (58)$$

holds for all test functions $v\in\mathcal{F}$, where

$$\mathcal{F}=\left\{\phi\in C^1(\bar{\Omega}_\tau):\frac{\partial^2\phi}{\partial x_i\partial x_j}\in C(\bar{\Omega}_\tau),\ \phi(r,z,\tau)=0,\ \phi(r,\psi+H,t)=0,\ \phi\to 0 \text{ as } z\to-\infty\right\}.$$

Theorem 2

1. A classical solution is also a weak solution.
2. If $\{\theta,\ E\}$ is a weak solution and there is a function S such that (40), (A) and (B) hold, then $\{\theta,\ S\}$ is a classical solution.

The proof is similar to the proof of Theorem 1. The discretisation of (38), $(39)_2$, $(41)_2$, (42), (51), (56) and (57) may converge to the weak solution of the splashing model as the mesh size tends to zero; further investigation of this being required.

6 Summary

Three mathematical models have been introduced to describe solidification and splashing in laser percussion drilling. The physical problem is flow between two unknown moving boundaries. In order to make the problem more tractable the following assumptions are made concerning the fluid flow (i) incompressible, (ii) axisymmetric, (iii) inviscid and (iv) negligible surface tension and gravity. The flow is also taken to be laminar and irrotational in the first model. This first model for laminar and irrotational flow is employed to derive a second averaged model. The second model is proposed for the possibility of turbulent flow.

The second model is derived from the first in the limit of small aspect ratio and large Stefan number for vaporisation. The resulting model is a combination of the shallow water equations in the zero gravity limit and a two-phase Stefan problem; the problem being reduced by obtaining a differential equation for the liquid/gas free surface. The thermal equation is the only field equation to remain from the first model. Shocks may occur. The accumulation of solidified material (recast) is considered to be related to shocks behind which the melt can amass. Therefore shocks are highly undesirable and may be avoided by ensuring that the melt velocity after the splash increases monotonically from the centre of the hole, that is the radial pressure gradients should become steeper towards the perimeter of the hole. This must be achieved by accurate control of the radial laser intensity profile. In the absence of shocks, other than the leading-edge shock, the resolidification will be in the form of thin layers. A key parameter group in the growth of the solidification is given by

$$\left(\frac{k}{\rho c}\right)^{1/2}\frac{c(T_m-T_a)}{L_f}.$$

As the material properties are usually fixed this highlights the importance of the difference between the melting and ambient temperatures and suggests experiments in which the metal target is heated prior to drilling. A heated target should suffer less from recast. Although heating may not be practical in commercial situations, reducing the time between pulses would have a similar effect.

A word of caution concerns the use of high laser intensity; in this régime only evaporation will take place. The resulting vapour will shield the metal surface by absorbing the laser radiation. A further word of caution regarding the use of high laser intensity concerns the increased probability of crack formation.

The last model modifies the second model by replacing the classical formulation of the energy equation with a weak formulation valid throughout the fluid, solid and at the fluid/solid interface. These weak formulations

are unusual because the fluid is moving across a solid surface. The weak formulation is far more amenable to numerical methods than the model in [6, 7] and is the first stage towards numerical calculations with the enthalpy method.

Acknowledgement

Financial support for this work was provided by the TMR contract entitled 'Differential Equations in Industry and Commerce'. This project has benefited from the generous advice of J. C. J. Verhoeven, J. K. M. Jansen, R. M. M. Mattheij, M. E. H. van Dongen, A. C. King and an anonymous referee.

References

[1] M. Allmen and A. Blatter, *Laser-Beam Interactions with Materials*, Springer-Verlag, Berlin, 1995.

[2] J. Dowden, M. Davis, and P. Kapadia, *Some aspects of fluid mechanics of laser welding*, J. Fluid Mech., 126 (1983), pp. 123–146.

[3] C. M. Elliott and J. R. Ockendon, *Weak and Variational Methods for Moving Boundary Problems*, Pitman Books Limited, London, 1982.

[4] A. C. Fowler, *Mathematical Models in the Applied Sciences*, Cambridge University Press, New York, 1997.

[5] M. C. Fowler and D. C. Smith, *Ignition and maintenance of subsonic plasma waves in atmospheric pressure air by cw CO_2 laser radiation and their effect on laser beam propagation*, J. Appl. Phys., 46 (1975), pp. 138–150.

[6] R. K. Ganesh and A. Faghri, *A generalized thermal modeling for laser drilling process–I. mathematical modeling and numerical methodology*, Int. J. Heat Mass Transfer, 40 (1997), pp. 3351–3360.

[7] ——, *A generalized thermal modeling for laser drilling process–II. numerical simulation and results*, Int. J. Heat Mass Transfer, 40 (1997), pp. 3361–3373.

[8] H. E. Huppert, *Phase changes following the initiation of a hot turbulent flow over a cold solid surface*, J. Fluid Mech., 198 (1989), pp. 293–319.

[9] I. E. Idelchik, *Flow Resistance: A design guide for engineers*, Taylor & Francis, Philadelphia, 1989.

[10] C. J. Knight, *Theoretical modeling of rapid surface vaporization with back pressure*, AIAA J., 17 (1979), pp. 519–523.

[11] L. D. Landau and E. M. Lifschitz, *Statistical Mechanics*, Pergamon, New York, 1980.

[12] H. W. Liepmann and A. Roshko, *Elements of Gas Dynamics*, John Wiley & Sons, New York, 1960.

[13] H. Ockendon and A. B. Tayler, *Inviscid Fluid Flows*, Springer-Verlag, New York, 1983.

[14] K. Ražnjević, *Handbook of Thermodynamic Tables and Charts*, Hemisphere, London, 1976.

[15] A. B. Tayler, *Mathematical Models in Applied Mechanics*, Oxford University Press, Oxford, 1986.

Appendix Gas Dynamics

The melt is ejected from the drilled hole by the radial pressure gradients generated by the sudden expansion of the vapour evaporating from the melt surface. The high recoil pressures involved also cause significant variation in the vaporisation temperature and rapid flow of vapour and air away from the melt surface. The following assumptions will be made (i) the time-scale of the gas dynamics is much smaller than the time-scale of the intensity variations, (ii) any beam/vapour interaction is negligible (the absorption coefficient of aluminium vapour is 0.5cm^{-1} at a temperature of 5000K [5] and a coaxial jet is employed to remove the aluminium vapour from the laser path), (iii) the vapour and air behave as ideal gases, (iv) there is no mixing between the aluminium vapour and compressed air, (v) the liquid-vapour interface has negligible width, (vi) all the laser energy is used to vaporise the melt, (vii) the three-dimensional problem can be viewed as an infinite set of one-dimensional problems parameterised by the intensity and (viii) the compression waves have coalesced to form discontinuities leaving the vapour and compressed air at constant pressure [12].

A schematic representation of the physical situation is shown in Figure 5, in which there are four regions [10]. The four regions are the ambient air, the compressed air, the metal vapour and the molten metal. These regions are separated by three interfaces: a shock between the ambient air ① and the compressed air ②, a contact surface between the compressed air ② and the metal vapour ③, and the liquid-vapour interface between the metal vapour ③ and the molten metal ④. Across the shock we have the Rankine-Hugoniot relations (see [13, p. 83])

$$\begin{aligned} \rho_1(U-u_1) &= \rho_2(U-u_2), && (59)\\ p_1+\rho_1(U-u_1)^2 &= p_2+\rho_2(U-u_2)^2, && (60)\\ c_1T_1+\frac{1}{2}(U-u_1)^2 &= c_2T_2+\frac{1}{2}(U-u_2)^2, && (61) \end{aligned}$$

where U is the shock speed, p the pressure, ρ the density, u the velocity, T the temperature, c the specific heat capacity at constant pressure and the subscripts denote the region of interest. Across the contact surface we have (see [12, p. 81])

$$p_2=p_3, \qquad u_2=u_3. \tag{62}$$

Let L_v denote the latent heat of vaporisation, I the laser intensity and c_v the specific heat capacity at constant volume of the melt. Across the liquid-vapour interface we have

$$\begin{aligned} \rho_4u_4 &= \rho_3u_3, && (63)\\ p_4+\rho_4u_4^2 &= p_3+\rho_3u_3^2, && (64)\\ \rho_4u_4\left(c_vT_4+\frac{1}{2}u_4^2+\frac{p_4}{\rho_4}\right)+I &= \rho_3u_3\left(c_3T_3+L_v+\frac{1}{2}u_3^2\right), && (65) \end{aligned}$$

representing conservation of mass, conservation of momentum and conservation of energy, respectively. We note that $\rho_3/\rho_4 \ll 1$, so that

$$u_4 \ll u_3, \qquad \rho_4u_4^2 \ll \rho_3u_3^2, \qquad \frac{1}{2}u_4^2 \ll \frac{1}{2}u_3^2, \qquad \frac{p_4}{\rho_4} \ll \frac{p_3}{\rho_3}.$$

We now use our assumption that all the laser energy is used to vaporise the melt, to obtain

$$I=\rho_4u_4L_v.$$

We deduce the leading-order expressions for the liquid-vapour interface

$$\rho_3u_3=\frac{I}{L_v}, \qquad p_3+\rho_3u_3^2=p_4, \qquad c_3T_3+\frac{1}{2}u_3^2=c_vT_4. \tag{66}$$

We must add three constitutive laws to close the system of equations. The metal vapour and the compressed air have been assumed to be ideal gases, which yields

$$p_2 = R_2 \rho_2 T_2, \qquad p_3 = R_3 \rho_3 T_3, \tag{67}$$

where R is the gas constant in the appropriate region. Across the liquid-vapour interface we use the Rankine-Kirchhoff equation

$$p_4(T_4) = p_4(T_{ref}) \left(\frac{T_4}{T_{ref}} \right)^{(c_3 - c_4)/R_3} \exp \left\{ \frac{L_0}{R_3} \left(\frac{1}{T_{ref}} - \frac{1}{T_4} \right) \right\}, \tag{68}$$

where the subscript ref corresponds to a reference state and $L_v = L_0 + (c_3 - c_4)T_4$. The Rankine-Kirchhoff equation is a first integral of the Clausius-Clapeyron equation [11]. The system to be solved consists of (59)–(62) and (66)–(68). The algebraic system of equations is solved with the routine C05NBF from the NAG library; the data being given in Table 3.

The recoil pressure as a function of intensity is shown in Figure 6. The radial pressure gradient can now be deduced from the known variation of intensity with radius. This is a necessary input to the splashing model. The high recoil pressure also causes the vaporisation temperature of the aluminium to vary considerably over this intensity régime (shown in Figure 7). This also has to serve as an input for the splashing model. In Figure 8 the different velocities as a function of intensity are sketched. The speed of sound in aluminium vapour is included to show that the compressed air speed or the speed of aluminium vapour is subsonic for the intensities of interest. This is in contrast to the assumptions in [6, 7]. The magnitude of these velocities with the typical length-scale ($\sim$ 1mm) allows us to determine the time-scale for the gas dynamics ($\sim 10^{-6}$s). The compressed air density is much larger than the density of the metal vapour (shown in Figure 9).

Symbol	Definition	Value
ρ	density	2.7×10^3 kg m $^{-3}$
$L_v(T_v)$	latent heat of vaporisation	1.2×10^7 J kg^{-1}
L_f	latent heat of fusion	3.6×10^5J kg^{-1}
k	thermal conductivity	2.3×10^2 W m^{-1}K^{-1}
c	specific heat capacity	9.0×10^2 J kg^{-1}K^{-1}
T_m	melting temperature	9.3×10^2K
T_v	vaporisation temperature	2.5×10^3 K
μ	viscosity	2.7×10^{-3} Pa s
σ	surface tension	1 kg s^{-2}

Table 1: Physical data for drilling aluminium

Symbol	Definition	Typical Value
δ	d/L	0.1
D	$k/\rho cUL\delta^2$	0.2
λ_f	$L_f/c(T_v - T_m)$	0.3
λ_v	$L_v(T_v)/c(T_v - T_m)$	8
$\bar{T}_a$	$(T_a - T_m)/(T_v - T_m)$	-0.4

Table 2: Dimensionless parameters for a typical laser percussion drilling process

Parameter	Value
R_1	3.0×10^2 N m kg^{-1} K^{-1}
R_2	3.0×10^2 N m kg^{-1} K^{-1}
R_3	3.1×10^2 N m kg^{-1} K^{-1}
c_1	1.0×10^3 J kg^{-1} K^{-1}
c_2	1.0×10^3 J kg^{-1} K^{-1}
c_3	5.0×10^2 J kg^{-1} K^{-1}
c_{p4}	1.0×10^3 J kg^{-1} K^{-1}
c_v	1.0×10^3 J kg^{-1} K^{-1}
$L_v(T_{ref})$	1.2×10^7 J kg^{-1}
T_{ref}	2.5×10^3 K
$p_4(T_{ref})$	1.2×10^5 N m^{-2}
u_1	0.0 m s^{-1}
p_1	1.0×10^5 N m^{-2}
T_1	3.0×10^2 K

Table 3: Physical data for aluminium vaporisation.

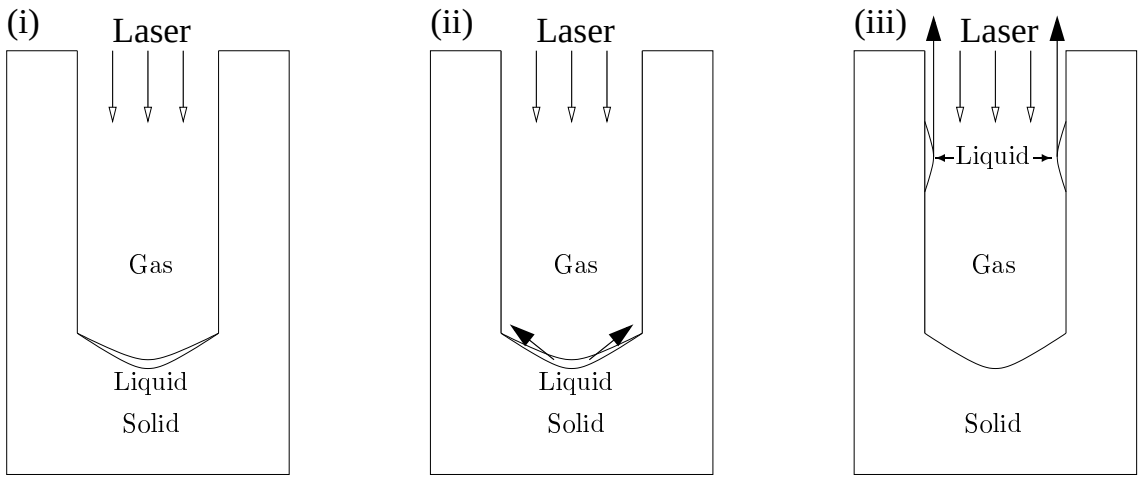

Figure 1: A schematic of the three stages in laser percussion drilling (i) melt-pool formation at the base of the drilled hole, (ii) splashing of the melt pool away from the axis of the drilled hole and (iii) solidification of the molten metal as it moves along the side wall. The filled arrows represent fluid motion and the unfilled arrows laser energy.

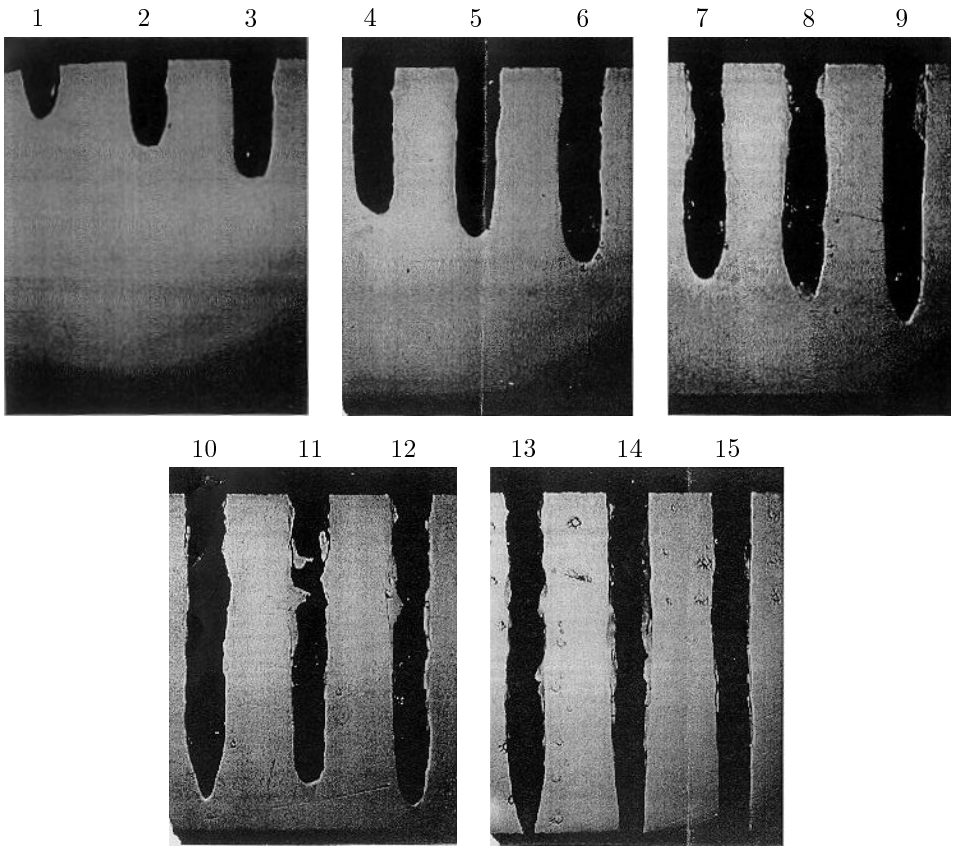

Figure 2: A series of photographs of holes produced by laser percussion drilling. The number of pulses to produce each hole is indicated (Courtesy of Eldim BV).

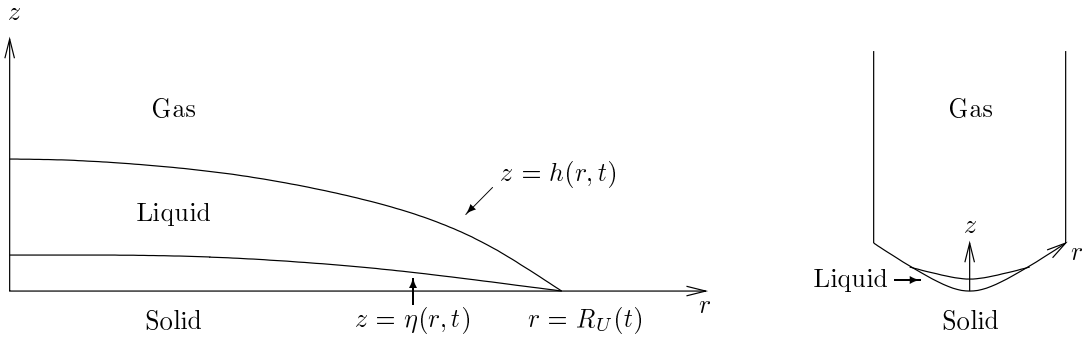

Figure 3: On the left the axisymmetric representation of splashing and on the right its interpretation on a drilled hole. The radial direction is denoted by r and the vertical direction by z. The incompressible fluid is in the region $0 < r < R_U(t)$ and $\eta(r,t) < z < h(r,t)$, and the solid is in the region $z < \eta(r,t)$.

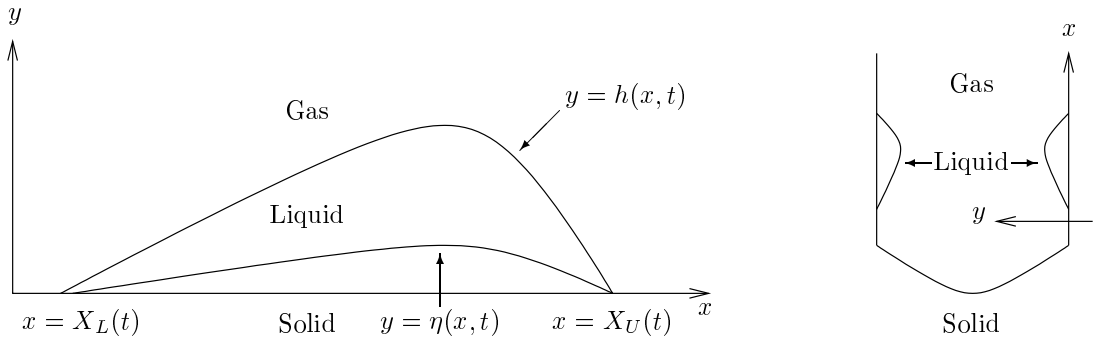

Figure 4: On the left the planar representation of solidification and on the right its interpretation on a drilled hole. The horizontal direction is denoted by x and the vertical direction by y. The incompressible fluid is in the region $X_L(t) < x < X_U(t)$ and $\eta(x,t) < y < h(x,t)$, and the solid is in the region $y < \eta(x,t)$.

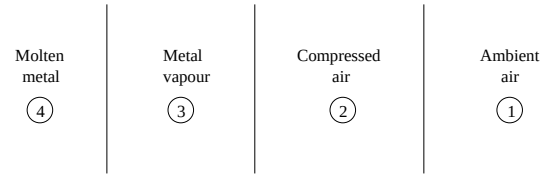

Figure 5: A schematic of the gas dynamics.

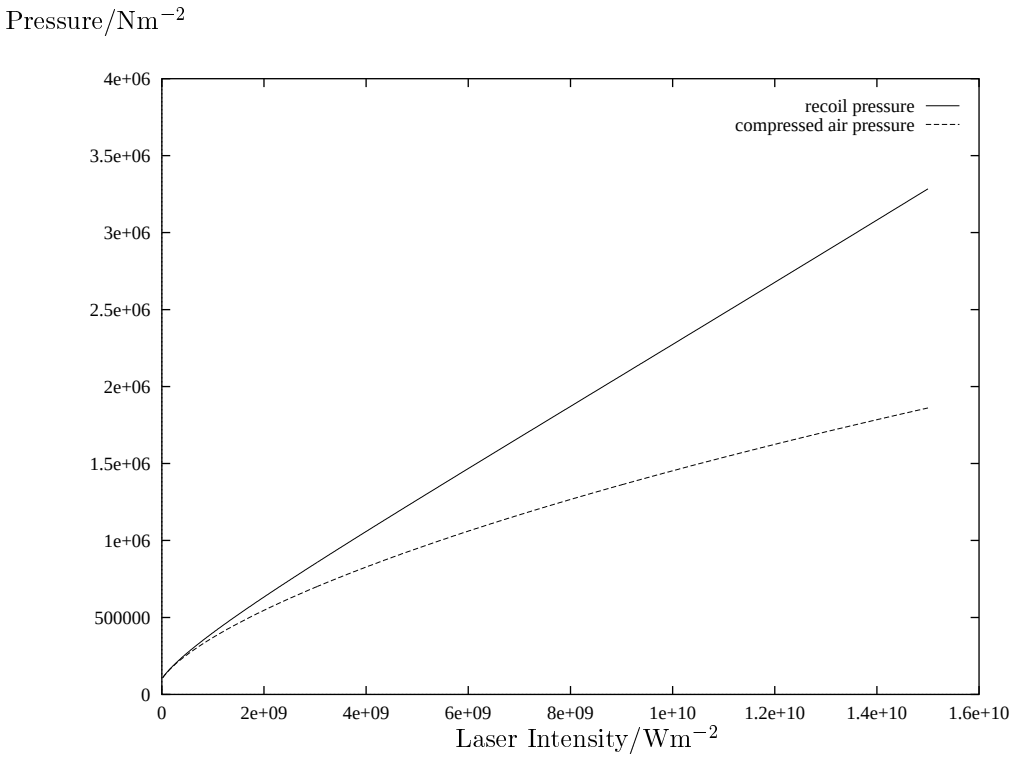

Figure 6: The recoil pressure and compressed air pressure as a function of laser intensity. The data is given in Table 3.

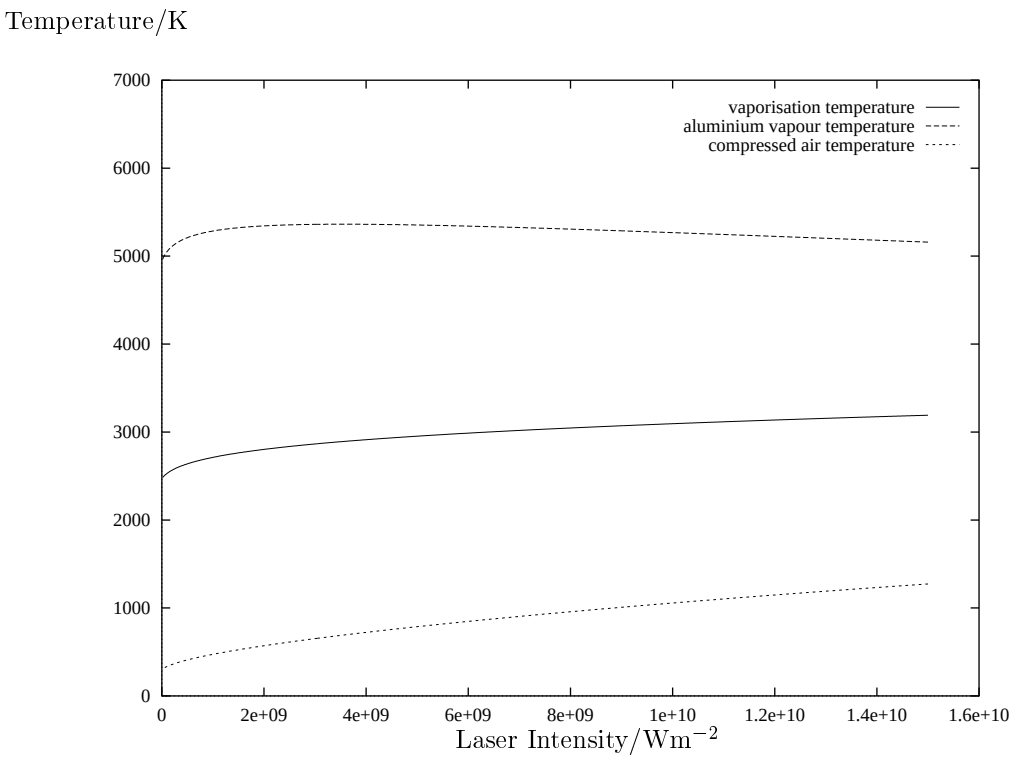

Figure 7: The vaporisation temperature, aluminium vapour temperature and compressed air temperature as a function of laser intensity. The data is given in Table 3.

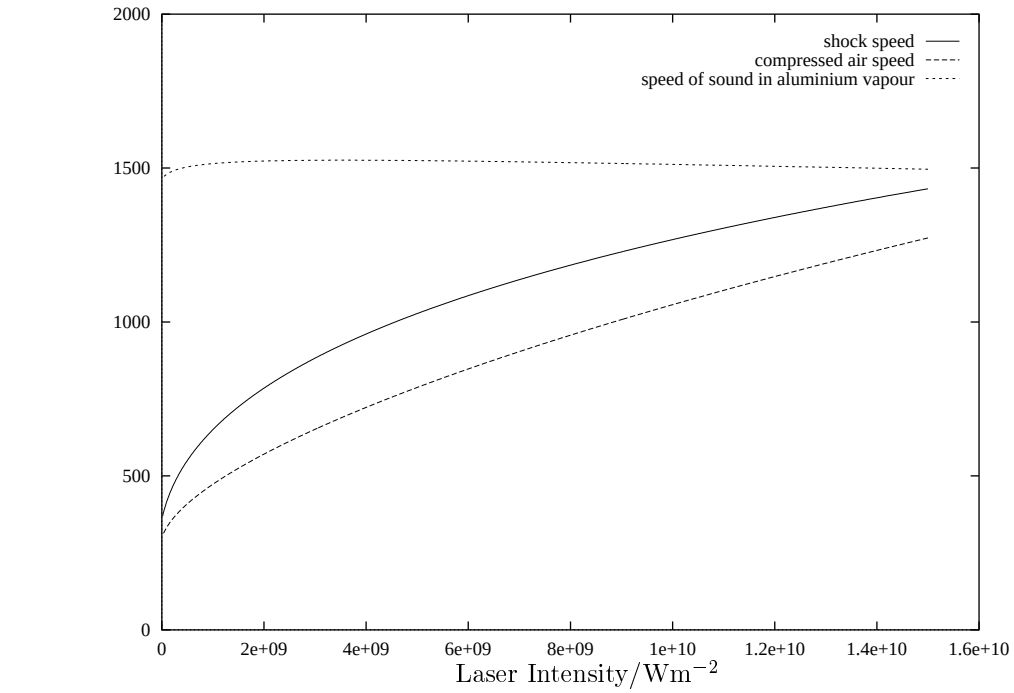

Figure 8: The shock speed, compressed air speed and speed of sound in the aluminium vapour as a function of laser intensity. The data is given in Table 3.

Density/kgm^{-3}

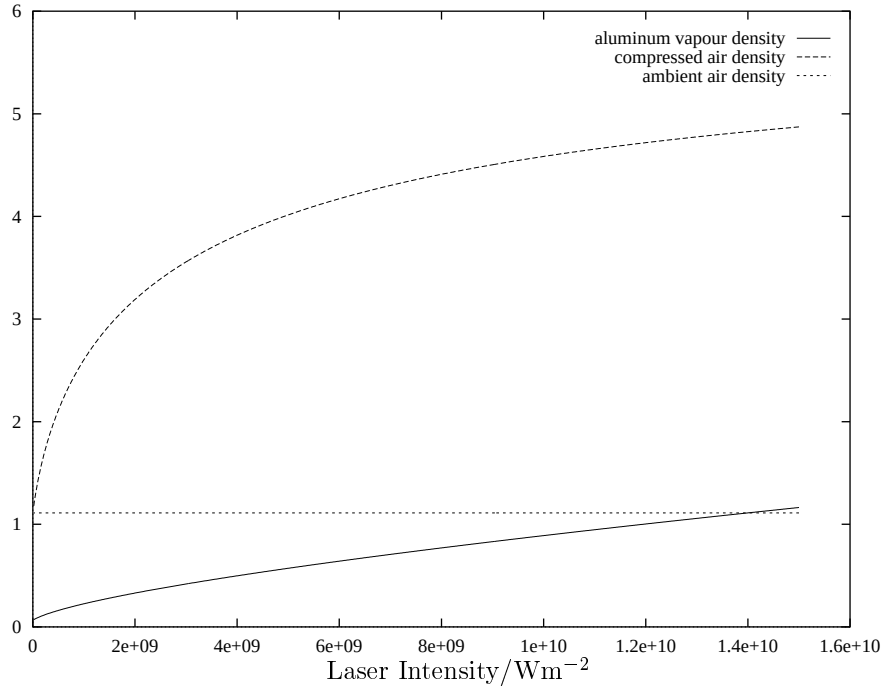

Figure 9: The aluminium vapour density, compressed air density and ambient air density as a function of laser intensity. The data is given in Table 3.